Special Issue

# Activated Retinal Pigment Epithelium, an Optical Coherence Tomography Biomarker for Progression in Age-Related Macular Degeneration

Christine A. Curcio,[1] Emma C. Zanzottera,[2] Thomas Ach,[3] Chandrakumar Balaratnasingam,[4,5] and K. Bailey Freund[6–8]

[1]Department of Ophthalmology, University of Alabama School of Medicine, Birmingham, Alabama, United States
[2]Eye Clinic, Department of Clinical Science "Luigi Sacco," Sacco Hospital, University of Milan, Milan, Italy
[3]University Hospital Würzburg, Department of Ophthalmology, Würzburg, Germany
[4]Center for Ophthalmology and Visual Sciences, Lions Eye Institute, University of Western Australia, Perth, Australia
[5]Sir Charles Gairdner Hospital, Perth, Australia
[6]Vitreous Retina Macula Consultants of New York, New York, New York, United States
[7]LuEsther T. Mertz Retinal Research Center, Manhattan Eye, Ear, and Throat Institute, New York, New York, United States
[8]Department of Ophthalmology, New York University Langone School of Medicine, New York, New York, United States

Correspondence: Christine A. Curcio, Department of Ophthalmology, EyeSight Foundation of Alabama Vision Research Laboratories, 1670 University Boulevard, Room 360, School of Medicine, University of Alabama at Birmingham, Birmingham, AL 35294-0099, USA; curcio@uab.edu.

Submitted: March 15, 2017
Accepted: June 4, 2017

Citation: Curcio CA, Zanzottera EC, Ach T, Balaratnasingam C, Freund KB. Activated retinal pigment epithelium, an optical coherence tomography biomarker for progression in age-related macular degeneration. *Invest Ophthalmol Vis Sci*. 2017;58:BIO211–BIO226. DOI:10.1167/iovs.17-21872

**Purpose.** To summarize and contextualize recent histology and clinical imaging publications on retinal pigment epithelium (RPE) fate in advanced age-related macular degeneration (AMD); to support RPE activation and migration as important precursors to atrophy, manifest as intraretinal hyperreflective foci in spectral-domain optical coherence tomography (SDOCT).

**Methods.** The Project MACULA online resource for AMD histopathology was surveyed systematically to form a catalog of 15 phenotypes of RPE and RPE-derived cells and layer thicknesses in advanced disease. Phenotypes were also sought in correlations with clinical longitudinal eye-tracked SDOCT and with ex vivo imaging–histopathology correlations in geographic atrophy (GA) and pigment epithelium detachments (PED).

**Results.** The morphology catalog suggested two main pathways of RPE fate: basolateral shedding of intracellular organelles (apparent apoptosis in situ) and activation with anterior migration. Acquired vitelliform lesions may represent a third pathway. Migrated cells are packed with RPE organelles and confirmed as hyperreflective on SDOCT. RPE layer thickening due to cellular dysmorphia and thick basal laminar deposit is observed near the border of GA. Drusenoid PED show a life cycle of slow growth and rapid collapse preceded by RPE layer disruption and anterior migration.

**Conclusions.** RPE activation and migration comprise an important precursor to atrophy that can be observed at the cellular level in vivo via validated SDOCT. Collapse of large drusen and drusenoid PED appears to occur when RPE death and migration prevent continued production of druse components. Data implicate excessive diffusion distance from choriocapillaris in RPE death as well as support a potential benefit in targeting drusen in GA.

Keywords: retinal pigment epithelium, age-related macular degeneration, optical coherence tomography, drusen, hyperreflective foci, transdifferentiation, apoptosis, migration, Mie scattering, electron microscopy, stereology

Age-related macular degeneration (AMD) is a major cause of global vision loss.[1] The visual consequences of neovascularization in AMD can be stabilized with regular antivascular endothelial growth factor therapy.[2] In contrast, geographic atrophy (GA), the end stage of nonneovascular AMD, is a degenerative process of the photoreceptor support system (retinal pigment epithelium [RPE] and choroid) that has no approved treatment or prevention.[3] AMD pathology exhibits intricate yet organized tissue layers that are yielding to persistent laboratory investigation and that can be appreciated, remarkably, in clinical spectral-domain optical coherence tomography (SDOCT).[4–6]

Project MACULA (http://www.projectmacula; in the public domain) is a National Eye Institute and foundation-funded online resource of human AMD histology that enabled detailed examination of features visible clinically through SDOCT such as subretinal drusenoid deposit[7] and outer retinal tubulation.[8,9] Here we summarize and contextualize recent histology and clinical imaging publications on RPE fate in nonneovascular AMD based on this resource.[6,10–18] Extensive SDOCT and histopathology literature was cited in our primary papers to create a unified system of RPE cellular morphology. In this review, our central thesis is that an accurate, cellular-level description of GA natural history is possible with optimized

structural SDOCT of RPE. We propose that activated, migrating RPE cells are a pathway to atrophy and the basis of one class of intraretinal hyperreflective foci, a progression biomarker. We also consider another class of hyperreflective foci thought to represent microglia, as described in neovascular disease.[12,19,20] Coupled with new information about how soft drusen form, histologically validated SDOCT imaging provides a clearer view of how RPE cells die in association with drusen to initiate GA.

The RPE is a monolayer of cuboidal polygonal cells embedded between photoreceptors and Bruch's membrane. Strong apical to basolateral polarization makes the RPE a key player in maintaining homeostasis of photoreceptors apically and choriocapillaris basally. Human RPE cells contain abundant organelles of imaging significance including lipofuscin, melanolipofuscin, melanosomes, and mitochondria. Autofluorescence and reflectivity of these organelles allow RPE visualization in laboratory and clinical settings. RPE cell location (e.g., foveal versus extrafoveal), morphology, and intracellular granule distribution may impact autofluorescence and reflectivity, thereby altering clinical fundus autofluorescence (FAF) and reflectivity (SDOCT) patterns. In AMD, RPE cells are instigators by producing extracellular deposits, reporters of still-invisible events in Bruch's membrane, victims that eventually succumb, and treatment targets.

SDOCT is an interferometry technique using reflections of low-coherence light to achieve depth-resolved, comprehensive, and noninvasive cross-sectional and en face views of chorioretinal structure.[3,21,22] Currently, SDOCT anchors a multimodal imaging approach (color photographs, dye-based and OCT angiography, near-infrared reflectance, and FAF),[3,23] which brings advantages of each individual technique to bear on single questions, deepening our understanding of pathology.

Just as histology helped energize single-cell outer retinal imaging,[24–28] linking SDOCT signals to cell and tissue features via histologic image validation can increase the accuracy and utility of this modality.[29–33] Histologic validation of SDOCT using animal models lacking a macula,[34–38] while informative, cannot elucidate structures and pathology unique to human retina. The few human eyes used to validate OCT[39–42] prior to our current work included little pathology, nonmacular tissues, categorically specified macular locations, or low-resolution OCT images.

Our approaches to OCT validation included a literature-based model of outer retinal anatomy,[43] quantitative high-resolution histology of short postmortem donor eyes at precisely defined macular locations, parallel case series of histology and clinical SDOCT, imaging–histology comparisons using ex vivo OCT, and direct clinicopathologic correlation in one AMD case with superb clinical documentation.

Clinicopathologic correlation[44] and epidemiology studies using color fundus photography[45–47] show that hyperpigmentation is a risk factor for progression to late AMD that quantitatively rivals drusen. In OCT, discrete intraretinal hyperreflective foci with underlying shadowing attached to RPE overlying drusen[21,48–50] were attributed to anteriorly migrated RPE by referring to similar foci seen in proliferative vitreoretinopathy, where RPE involvement was known.[51] Foci were also correlated with hyperpigmentation,[52,53] thus linking to knowledge of AMD progression available from population-based epidemiology.[45–47] Foci could be found as far inward as the ganglion cell layer, but more often in photoreceptor layers.[53,54] Using eye-tracked SDOCT to track 571 individual drusenoid lesions, Ouyang et al.[54] found that progression risk factors included the presence of hyperreflective foci at baseline, with inward movement of foci over time[55] conferring the greatest risk (odds ratio, 28.2). In a recent SDOCT-based risk calculator for progression to GA,[56] hyperreflective foci are one of four major indicators, along with total drusen volume,[57] development of internal hyporeflectivity within drusen,[54,55] and the presence of subretinal drusenoid deposits.[58]

## Methods

### The Project MACULA Web Site of AMD Histopathology

Population-based eye pathology is made possible by a 25-year collaboration with the Alabama Eye Bank, which has high volume for transplantable tissues and the fastest tissue recovery time among US eye banks. Between 1996 and 2010, our laboratory accessioned >900 pairs of nondiabetic donor eyes within 4 hours (before 2001) or 6 hours (after 2001) of death. In 2010, federal and private funding enabled creation of the Project MACULA Web site as a resource for clinical imaging, using 142 maculas (53 advanced AMD, 13 GA eyes from 12 donors and 40 neovascular AMD eyes from 40 donors; 29 early AMD; 60 age-matched control eyes). Prior to histology, all eyes were subjected to ex vivo imaging including color fundus photography using a dissecting microscope with epi- and oblique transillumination, and SDOCT using a custom tissue holder for a Spectralis HRA+OCT (Heidelberg Engineering, Heidelberg, Germany).[12] This holder holds a donor eye lacking an anterior segment, so that the fundus looks horizontally into the instrument through a 60-diopter lens, thus emulating clinical imaging. Tracking from scans obtained during a donor's lifetime can be used to align macular specimens after death. Thus, SDOCT has become essential for the pathology laboratory.

Because contemporary SDOCT provides exquisite structural detail, clinical interpretation is best served by morphologic descriptions that are comprehensive, quantitative, pegged to precise retinal locations, and digitally available. Thus, we sought views that were high magnification, high resolution, color, and panoramic, with the original histology accessible online. Transmission electron microscopy, a comprehensive visualization technique, reveals all organelles including spindle-shaped melanosomes unique to RPE. Submicrometer-thick sections of epoxy resin blocks can emulate the benefits of low-magnification color electron microscopy over wide tissue samples. Postfixation with osmium tannic acid paraphenylenediamine (OTAP) preserves extracellular lipids[59–62] and imparts polychromaticity to toluidine blue–stained sections. We surveyed standard locations in superior and central macula (through rod ring and foveola, respectively).[24] At 25 locations in central sections and 13 locations in superior sections (1050 locations per eye; >150,000 total for all eyes), 21 chorioretinal layers were measured and RPE morphology was annotated with a custom ImageJ (https://fiji.sc/; in the public domain) drop-down menu. Systematic sampling enabled unbiased estimates of phenotype frequency.

### RPE Visibility in SDOCT, In Vivo and Ex Vivo

High RPE reflectivity on SDOCT facilitates the investigation of cell fate. Reflectivity in OCT corresponds to the scattering of light as it travels through inhomogeneous media having interfaces of varying refractive index. Organelles contribute reflectivity, because light scatters off refractive index boundaries according to the physical principle of Mie scattering. Of organelles, mitochondria and lysosomes are the major scatterers.[63–65] The RPE has three stacked cushions of

Investigative Ophthalmology & Visual Science

organelles, melanosomes apically, lipofuscin and melanolipofuscin granules (of lysosomal origin) in midcellular regions, and mitochondria basally. RPE also strongly shadows posterior structures, such as basal laminar deposit (BLamD) in AMD, which then may be uncovered by RPE loss. In our survey, we used the presence of melanosomes, lipofuscin granules, and (extracellular) BLamD as anatomic markers for RPE. Further, in human donor eyes preserved ≤6 hours after death, the ocular fundus retains many of its in vivo SDOCT imaging characteristics.[12,16]

A comprehensive clinical lexicon for chorioretinal anatomy in SDOCT[66] uses the term RPE–Bruch's membrane band for the outermost of the four outer retinal reflective bands. We suggested[67] that this band in normal eyes be called RPE–basal lamina (BL)–Bruch's membrane (RBB) to accommodate drusen, neovascular membranes, cells, hemorrhage, and fluid that accumulates between the RPE-BL and the inner collagenous layer in AMD eyes. In SDOCT descriptions, we use the term RPE-BL for the band created by the separation of RPE and either its BL or BLamD from Bruch's membrane.[14] In histology descriptions, we use the terms RPE-BL or RPE-BLamD, as appropriate.

## Review of Published Results

### Catalog of RPE Morphology in Histology and SDOCT

A major outcome of Project MACULA was an extensive catalog of RPE morphology, and with it, new insight into the precursors of atrophy. We hypothesized that the RPE exhibits stereotypic stress responses and death pathways that could be defined, quantified, and followed over time. Cellular fates included death, transdifferentiation to a cell type not recognizable as RPE, and emigration. We expanded our previous system of morphologic phenotypes.[68,69] Prior histologic descriptions, including our own, were fragmentary, due to use of low magnification, or low-resolution tissue preparation and photomicroscopy, small sample size, insufficiently advanced disease, and nonquantitative descriptors of morphology and retinal position. The benefit of our new approach, if successful, was visualization targets and metrics for clinical trials and practices using eye-tracked SDOCT as sources of longitudinal data.

In late atrophic and neovascular AMD maculas, we defined 15 histologic phenotypes, ranging from age normal to total absence of RPE and its basal lamina (illustrated, Fig. 1; survey results, Supplementary Table). Of these phenotypes, 10 were epithelial (contacting or near basal lamina), 3 were RPE derived (no contact with basal lamina), and 2 were atrophic (no cells). All but two were found in both end stages, thereby justifying one system. To help focus future research, we sought major trends in the survey results. Prominent phenotypes were dissociated RPE cells in the atrophic zone, shedding cells that drop granule aggregates into the underlying BLamD, sloughed cells in the subretinal space, intraretinal cells within the neurosensory retina, and subducted cells between the RPE-BL and the inner collagenous layer of Bruch's membrane (Figs. 1G, 1E, 1I, 1F, 1D, respectively). In separate studies using ex vivo OCT,[15,18] we found that diffuse hyperreflectivity on the inner aspect of the RPE-BL band corresponded to RPE organelles extruded into the subretinal space and mixed with outer segment debris (vitelliform phenotype) (Fig. 1C). Two RPE phenotypes seen in neovascular AMD eyes only were entombed cells trapped within scars (Fig. 1J) and melanotic cells (Fig. 1H), derived from entombed, with spherical melanosomes imparting black pigmentation to the fundus. In advanced AMD, surviving cone photoreceptors are scrolled into outer retinal tubulation[8,70] and in the lumens are free-floating RPE, that is, sloughed cells that drift in from outside the atrophic area (entubulated, Fig. 1K).

These results suggested two main pathways of RPE fate in advanced AMD. One pathway comprised the shedding of pigmented and autofluorescent granule aggregates into BLamD (shedding phenotype; Fig. 1E), which appears apoptotic. As shown in flat-mounted AMD retinas,[11] aggregates 5 to 20 μm in diameter originate within RPE cell bodies that are overall degranulating. A second pathway comprised the rounding and sloughing of cells into the subretinal space with anterior migration into the neurosensory retina (sloughed and intraretinal phenotypes, Figs. 1I, 1F). The net effect of cells dying and leaving is that the RPE layer eventually breaks up into dissociated cells, and atrophy ensues (Fig. 1G). In the atrophic zone, some dissociated cells subduct, flatten, and migrate into the perilesional area (Fig. 1D). Dissociated cells are a logical precursor of subducted, because they are already released from junctional complexes; transitional morphologies between dissociated and subducted are found in single continuous histologic sections; subducted is disproportionately found in the atrophic area (Supplementary Table), and there is no obvious source in nonatrophic retina.

With this knowledge of RPE morphology and distribution, one can now recognize at least nine phenotypes in high-quality structural SDOCT (Fig. 2). Other phenotypes are likely also visible but have not yet been actively sought. Circular highly reflective foci correspond to sloughed and intraretinal phenotypes (Figs. 2B–C). A diffuse subretinal reflectivity corresponds to vitelliform (Fig. 2D). Granule aggregates of the shedding phenotype, despite their small size, were directly correlated to small reflective spots within thick BLamD of a patient who had been imaged 8 months before death[6] (Fig. 2E). In atrophic areas, reflective spots suggesting dissociated cells (Fig. 3F) can be distinguished from the absence of punctate reflectivity along Bruch's membrane (atrophy without BLamD, Fig. 3I). RPE atrophy with BLamD, that is, persistent BLamD, presents SDOCT signatures of outer retinal corrugations,[4] or if large, plateaus[71] (Fig. 3H), following the resolution of drusen or neovascularization. Small reflectivities under plateaus may represent subducted RPE, hydroxyapatite formations, or as yet unidentified components of reactive Müller cell processes, which are abundant in this region (Fig. 3H). These reflectivity sources remain to be characterized. The timing of plateau formation will be discussed in the section on timing and mechanism of RPE activation with respect to the drusen life cycle.

### RPE Morphologies at the Border of Atrophy

The defining contribution on GA was the epic description by Sarks et al.[72] of the transition to atrophy in five eyes prepared for panoramic transmission electron microscopy, backed by a 208-patient clinical series. This classic study revealed pigment clumping, loss of pigment, heterogeneity of cell sizes and shapes, formation of multiple layers, and presence of pigmented cells in the subretinal and sub-RPE space, with changes more prominent in the junctional zone than elsewhere.

We recently confirmed and quantified this progressive RPE dysmorphia in two sets of eyes (Fig. 3A).[10,17] A pathogenic sequence is proposed in Figure 4. In GA, the limits of atrophy in the photoreceptor layers are defined by a curved line[73] where the external limiting membrane (ELM) descends to

Investigative Ophthalmology & Visual Science

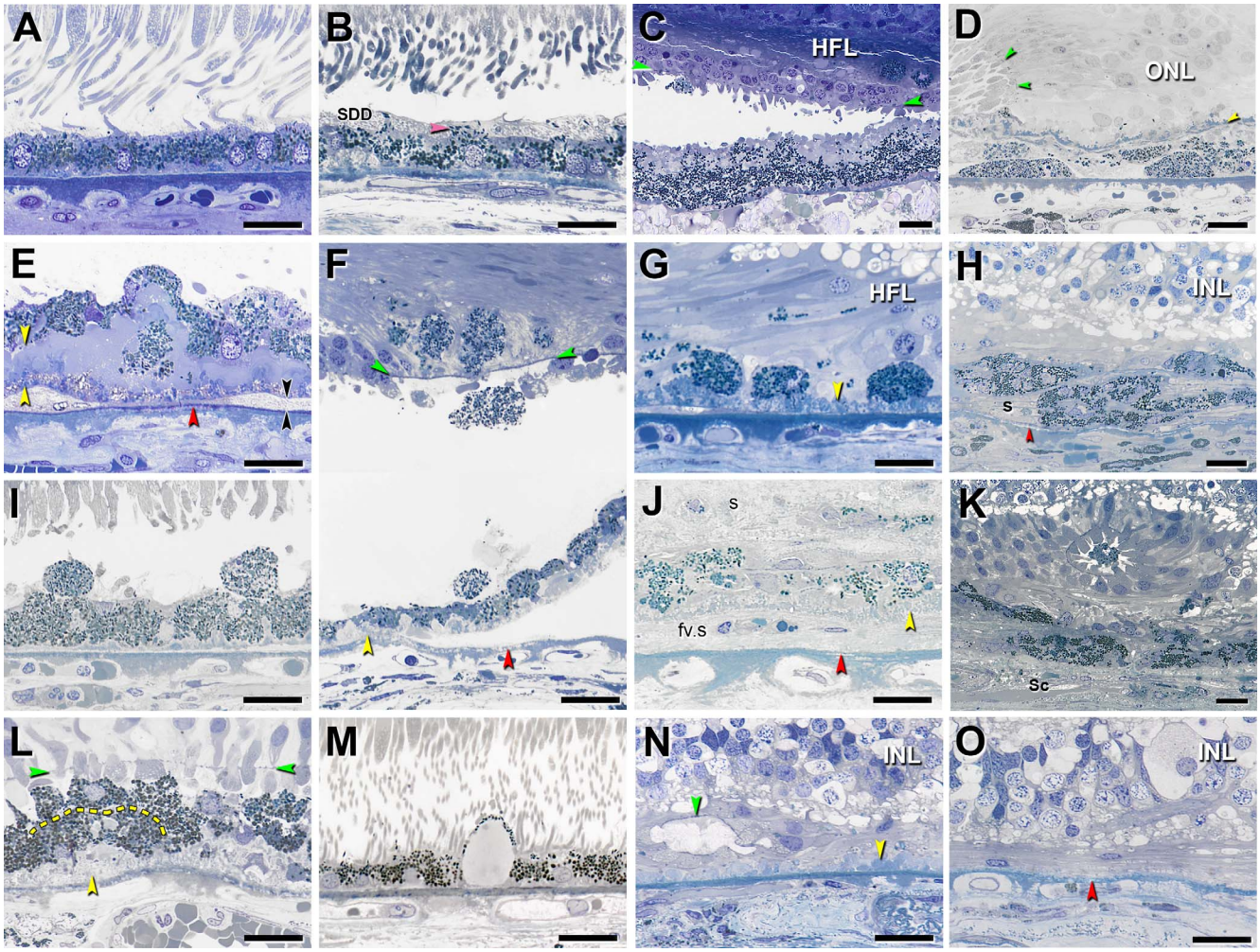


**Figure 1.** Fifteen phenotypes of retinal pigment epithelial cell morphology in advanced age-related macular degeneration. Assembled from previous descriptions.[6,8,13,15,18] Submicrometer epoxy resin sections of OTAP-postfixed specimens were stained with toluidine blue. *All scale bars* are 20 μm. Abbreviations: BLamD, basal laminar deposits; BLinD, basal linear deposits; ELM, external limiting membrane; HFL, Henle fiber layer; INL, inner nuclear layer; RPE, retinal pigment epithelium. *Yellow arrowheads*: BLamD; *red arrowheads*: calcification in Bruch's membrane; *green arrowheads*: ELM. (**A**) "Nonuniform" RPE: slightly nonuniform morphology and pigmentation with small patches of early BLamD. (**B**) "Very Nonuniform" RPE: highly nonuniform in shape and pigmentation; *pink arrowhead*: melanosomes within apical processes; SDD, subretinal drusenoid deposits. (**C**) "Vitelliform": exploded RPE lipofuscin/melanolipofuscin granules are mixed with outer segment debris. Intact RPE is also present in the HFL. (**D**) "Subducted": flattened cells with spindle-shaped melanosomes and lipofuscin/melanolipofuscin granules are located between persistent BLamD and Bruch's membrane. Border of atrophy is defined by a curved ELM. (**E**) "Shedding" RPE: basal translocation of granule aggregates into a thick continuous layer of BLamD; *black arrowheads*: BLinD. (**F**) "Intraretinal" RPE: anterior migration through ELM into the retina. Epithelial component remains atop BLamD (*bottom*). Photoreceptors have degenerated. Loss of soft druse contents and detachment of retina are artifacts. (**G**) "Dissociated" RPE: fully granulated and nucleated cells in the atrophic area, adherent to BLamD. Some RPE granules are translocated among HFL fibers. (**H**) "Melanotic": contain spherical polydisperse melanosomes and are located inside and internal to a sub-RPE fibrous scar(s) without BLamD, encapsulated by a light blue–staining collagenous material. (**I**) "Sloughed" RPE: spherical, fully granulated, nucleated cells released into the subretinal space. (**J**) "Entombed" by a subretinal scar (s) and a sub-RPE scar (fv.s). Persistent BLamD divides these compartments. (**K**) "Entubulated": nucleated RPE cell within the lumen of outer retinal tubulation, that is, cone photoreceptors surviving RPE degeneration, scrolled up by Müller cells. (**L**) "Bilaminar": two layers of fully pigmented cells delimited by *dotted line*, adherent to BLamD. (**M**) "Vacuolated" RPE: cells with a single large vacuole delimited by effaced cytoplasm. (**N**) "Atrophy with BLamD": absent RPE and persistent BLamD. Photoreceptors have atrophied. *Teal arrowhead*: ELM delimits end-stage outer retinal tubulation. (**O**) "Atrophy without BLamD": absent RPE, absent BLamD, absent photoreceptors. Glial scar and INL contact Bruch's membrane. (**A**, **B**, **E**–**G**, **I**, **J**, **L**–**O**) reprinted from Zanzottera EC, Messinger JD, Ach T, Smith RT, Freund KB, Curcio CA. The Project MACULA retinal pigment epithelium grading system for histology and optical coherence tomography in age-related macular degeneration. *Invest Ophthalmol Vis Sci*. 2015;56:3253–3268. © 2015 ARVO. (**C**) reprinted from Balaratnasingam C, Messinger JD, Sloan KR, Yannuzzi LA, Freund KB, Curcio CA. Histologic and optical coherence tomographic correlates in drusenoid pigment epithelium detachment in age-related macular degeneration. *Ophthalmology*. 2017;124:644–656. © 2017 by the American Academy of Ophthalmology. (**D**, **H**) reprinted from Zanzottera EC, Messinger JD, Ach T, Smith RT, Curcio CA. Subducted and melanotic cells in advanced age-related macular degeneration are derived from retinal pigment epithelium. *Invest Ophthalmol Vis Sci*. 2015;56:3269–3278. © 2015 ARVO. (**K**) reprinted from Schaal KB, Freund KB, Litts KM, Zhang Y, Messinger JD, Curcio CA. Outer retinal tubulation in advanced age-related macular degeneration: optical coherence tomographic findings correspond to histology. *Retina*. 2015;35:1339–1350. © 2015 by Ophthalmic Communications Society, Inc.

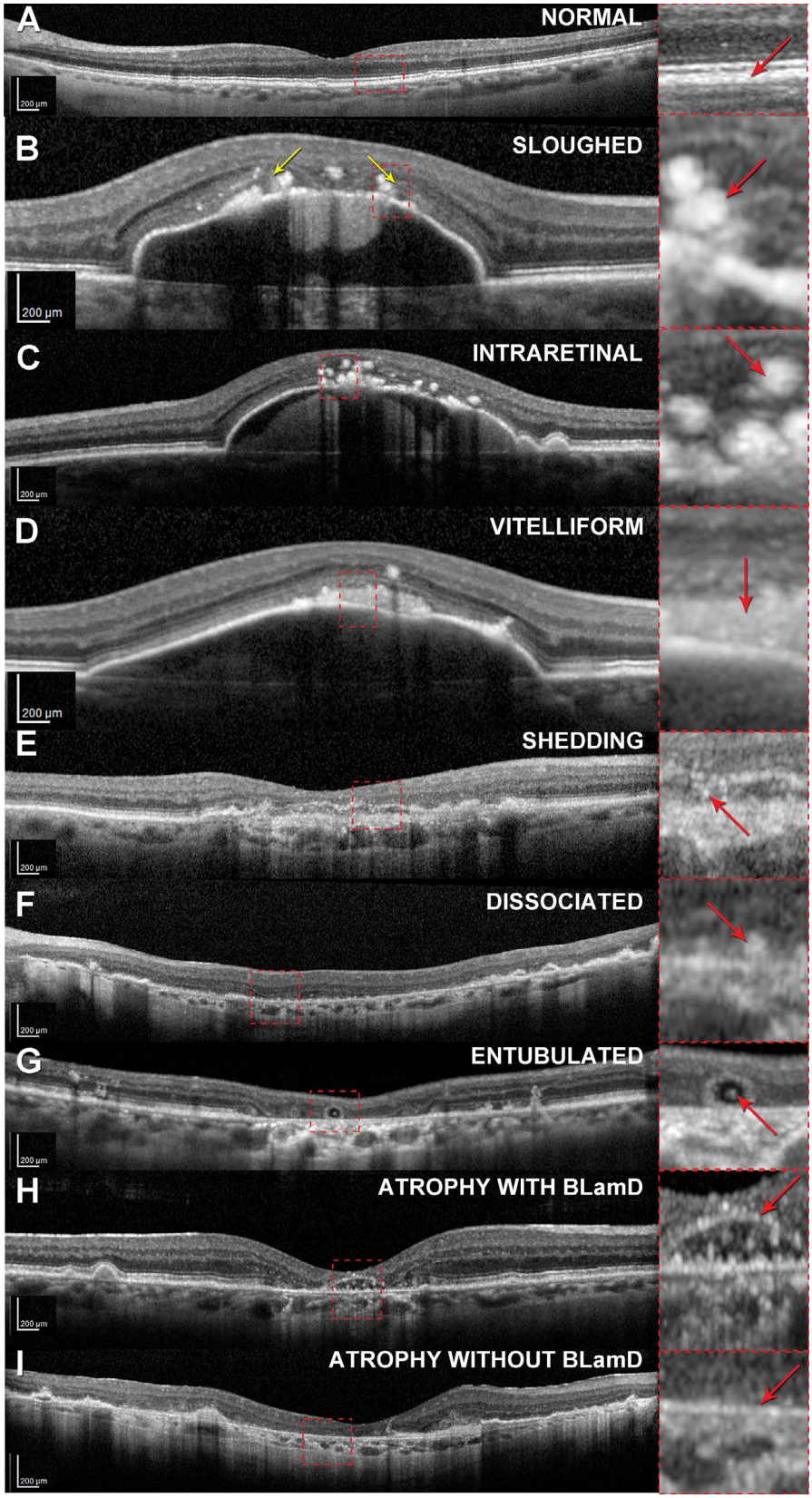


**Figure 2.** Retinal pigment epithelium phenotypes in spectral-domain optical coherence tomography. All images were captured on a Spectralis (Heidelberg Engineering, Heidelberg, Germany) using published protocols (**B–D**,[18] **E**, **H**[71]). (**G**) was provided courtesy of K. Litts and Y. Zhang.[130] (**B**, **D**) were acquired using 20° wide B-scans, and all others, 30° scans, as reflected in the *scale bars*. Eyes in (**B–D**, **F–I**) are nonneovascular AMD. The eye in (**E**) had neovascularization discovered in postmortem histopathology. In the panoramic scan of each phenotype (*left column*), a *dashed frame* delimits an area detailed in the *right column*. In the *right column*, *red arrows* indicate features corresponding to histologic phenotypes. Phenotypes from Figure 1 that are not included here have not yet been systematically sought. (**A**) Normal aged retina with slightly nonuniform RPE-

Investigative Ophthalmology & Visual Science

BL-Bruch's membrane band. (**B**) Sloughed cells (rounded and stacked) at the border of atrophy indicated by the descent of the ELM in a curved line (*yellow arrows*). (**C**) Intraretinal cells, also spherical. (**D**) Vitelliform material, comprising RPE organelles and outer segment debris. (**E**) Shedding of RPE granule aggregates into thick BLamD. The features are very small, because these are cellular fragments. (**F**) Dissociated cells are scattered across the atrophic area. (**G**) Individual RPE are found in the lumen of outer retinal tubulation, as are smaller non-RPE cells. The largest reflective features are presumed to be RPE. (**H**) Atrophy of RPE with persistent BLamD, which leaves a distinctive, raised hyperreflective line ("plateau") after the cells died or migrated away. See also Figure 8. (**I**) Atrophy of RPE without detectable BLamD.

Bruch's membrane (for OCT, Fig. 2B). We asked if RPE phenotypes distribute across the descent of the ELM in a manner consistent with the two-pathway hypothesis, that is, in a progression from normal to worse. In 13 GA eyes, we annotated RPE morphology and measured layer thicknesses at ±500 and 100 μm on either side of 69 ELM descents, for a total of 171 assessments chosen by unbiased sampling. Figure 3B graphically displays the frequency of RPE phenotypes on either side of this boundary, ranging from less affected at the top to more affected at the bottom. We found that proportions of sloughed and intraretinal RPE increase, and proportions of age-normal cells decrease, toward the ELM descent. In the atrophic zone, dissociated RPE were common, especially near the ELM descent, as were subducted cells, which were also present in reduced numbers in nonatrophic retina.

Progressive dysmorphia toward the ELM descent resulted in thickening of the combined RPE-BLamD layer by a statistically significant ~20%, although BLamD itself did not thicken. We contrast these findings for GA with those in 27 neovascular AMD eyes accessioned largely before the advent of intravitreal antivascular endothelial growth factor therapy in 2006. The transition to macular atrophy in neovascular AMD exhibited neither worsening of RPE nor thickening of the combined RPE-BLamD layer near the ELM descent,[16] consistent with the Sarks et al.[74] study using paraffin histology.

Hyperautofluorescence is considered an indicator for progression in GA, with different FAF patterns indicating different expansion rates.[75,76] Hyper-FAF can be explained by several cell-autonomous mechanisms, including increased concentration of efficiently detected fluorophores, increased concentration of intracellular lipofuscin granules, loss or repositioning of screening melanosomes, RPE dysmorphia resulting in taller individual cells, and RPE migration resulting in vertically superimposed cells. In 10 GA eyes, using unbiased sampling, confocal microscopy, and image analysis,[10] we determined that hyperautofluorescence was related to the path length for exciting light through fluorophores created by either enlarged and stacked RPE in the subretinal space or by autofluorescent granule aggregates within underlying BLamD. Because RPE dysmorphia is replicable,[10,17] it should be considered the leading explanation of focally increased FAF in GA, rather than high intracellular concentration of lipofuscin.

## Pigment Epithelium Detachment, a Defined Precursor to Atrophy

Pigment epithelium detachment (PED) is a defined precursor to atrophy in both GA and neovascular AMD.[72,77–81] PED forms include drusenoid, serous, vascularized, and mixed, some of which resolve with a legacy of RPE atrophy and vision loss. We

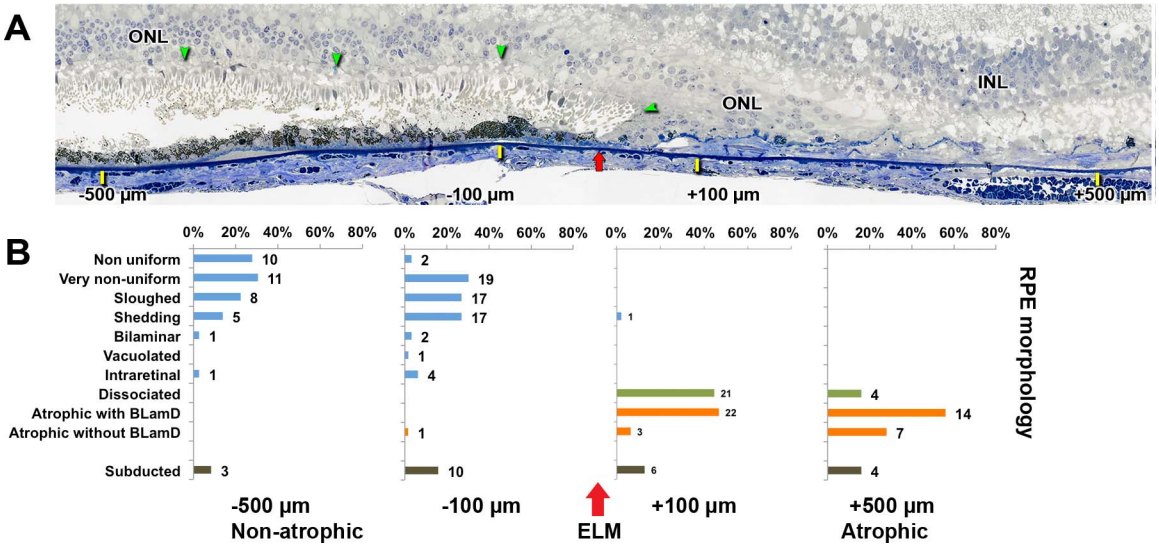


**Figure 3.** Progression of RPE phenotypes in the transition to geographic atrophy. (**A**) External limiting membrane descent (*green arrowheads*) and its projection onto Bruch's membrane (*red arrow*) are shown. RPE and BLamD morphology and thickness were analyzed at −500 and −100 mm outside GA (*yellow ticks*, to the *left of the red arrow*) and +500 and +100 mm inside GA (*yellow ticks*, to the *right of the red arrow*). Submicrometer epoxy section of OTAP-postfixed specimen, toluidine blue stain. INL, inner nuclear layer; ONL, outer nuclear layer. The ONL sweeps past a reflected ELM descent, into the atrophic area (90-year-old man). Adapted from Reference 17. (**B**) Distribution of RPE morphologies relative to the ELM descent in 13 GA eyes. The ELM descent defines GA margins (*red arrow*). The number of assessment locations is expressed at the *right of each bar*. Less affected morphology is at the *top* and more affected is at the *bottom*. Percentages are referenced to the total number of RPE. There is a shift from age-normal to abnormal RPE phenotypes close to (100 μm) the ELM descent. Dissociated RPE is prominent in the atrophic area, and subducted cells are found on both sides of the border. Reprinted from Zanzottera EC, Ach T, Huisingh C, Messinger JD, Spaide RF, Curcio CA. Visualizing retinal pigment epithelium phenotypes in the transition to geographic atrophy in age-related macular degeneration. *Retina*. 2016;36(suppl 1):S12–S25, with permission from Wolters Kluwer. © 2016 by Ophthalmic Communications Society, Inc.

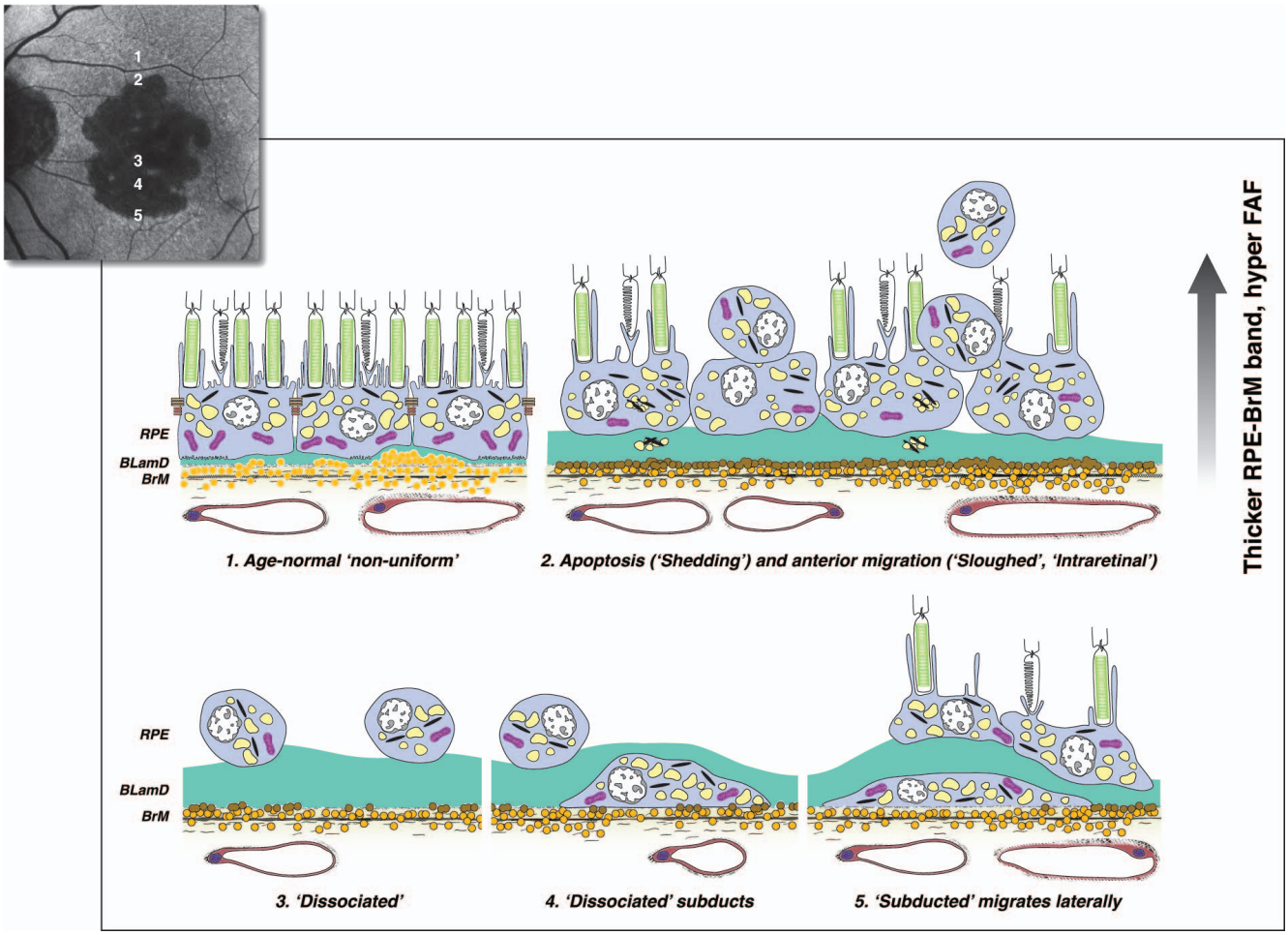


**Figure 4.** Hypothesized sequence of RPE fate, with imaging consequences, at the border of geographic atrophy in AMD. The ELM descent is not shown. As indicated on a representative FAF image of a patient with GA, (**1**–**2**) move from the margin of atrophy to its center. (**3**–**5**) move from the center to the margin. (**1**) Age-normal "nonuniform" RPE overlies Bruch's membrane, which contains numerous lipoprotein particles (*yellow*). Basal laminar deposit (*green*) is thin and continuous. (**2**) Within 500 μm of the border are "shedding" cells (perhaps apoptotic) and anteriorly migrating cells ("sloughed" and "intraretinal"). BLamD is thick. The imaging consequences of RPE dysmorphia are thickening and roughening of the hyperreflective RPE-BL-Bruch's membrane band by SDOCT, hyperreflective foci in the retina and within thick BLamD, and variably focal hyperautofluorescence. (**3**) Because of death or migration of RPE, the remaining layer disintegrates. "Dissociated" RPE are scattered across the atrophic zone and may be visible by autofluorescence. (**4**) "Subducted" cells likely originate in the atrophic zone, where they are unmoored from their junctional complexes. They dive down and flatten on Bruch's membrane while retaining a reduced number of characteristic granules. (**5**) "Subducted" cells migrate at least 100 μm into the marginal area and may express inflammatory markers. While their activities are yet to be learned, they could participate in the spread of GA. Reprinted from Zanzottera EC, Ach T, Huisingh C, Messinger JD, Spaide RF, Curcio CA. Visualizing retinal pigment epithelium phenotypes in the transition to geographic atrophy in age-related macular degeneration. *Retina*. 2016;36(Suppl 1):S12–S25, with permission from Wolters Kluwer. © 2016 by Ophthalmic Communications Society, Inc.

asked if we could observe cellular behavior in vivo and test the two-pathway hypothesis in drusenoid PED.

We first showed that ex vivo SDOCT correlates to histology in an exceptionally well-preserved donor eye.[18] In a 2-mm-diameter, large PED surrounded by soft drusen, we matched 30 high-resolution histology sections to 30 B-scans and accounted for all the hyperreflective features. Figure 5 shows representative paired scans and sections. In this eye, hypertransmission of light into the choroid represents an atrophic area containing dissociated RPE (Figs. 5A, 5B). Intraretinal hyperreflective foci with shadowing, varying in size, are fully pigmented, nucleated RPE cells, single and grouped (Figs. 5A–D). Among these foci, one distinctive signature ("RPE plume") represented grouped cells migrating anteriorly and turning 90° to track along the radiating Henle fibers. Also shown in Figures 5C and 5D is subretinal vitelliform material and sloughed RPE and intraretinal RPE in the outer nuclear layer (ONL). RPE were also found adjacent to capillaries, as far internal as the ganglion cell layer.

We then showed that almost all features observed in this ex vivo imaging–histology comparison were also visible by clinical SDOCT in drusenoid PED.[18] Paralleling the histology, a 48-case clinical series of drusenoid PED (≥2 mm diameter) was assembled. Cases were selected retrospectively from consecutive PED seen over a 6-month interval in one center and excluded eyes with choroidal neovascularization, other retinal diseases, and those receiving prior ocular therapies. Figure 6 shows that remarkably, optimized structural SDOCT revealed histologic detail about cellular behavior, including thickening of the RPE-BL band, spherical hyperreflective foci resembling single cells, irregular foci resembling groups of cells, and foci surrounding retinal capillaries.

Investigative Ophthalmology & Visual Science

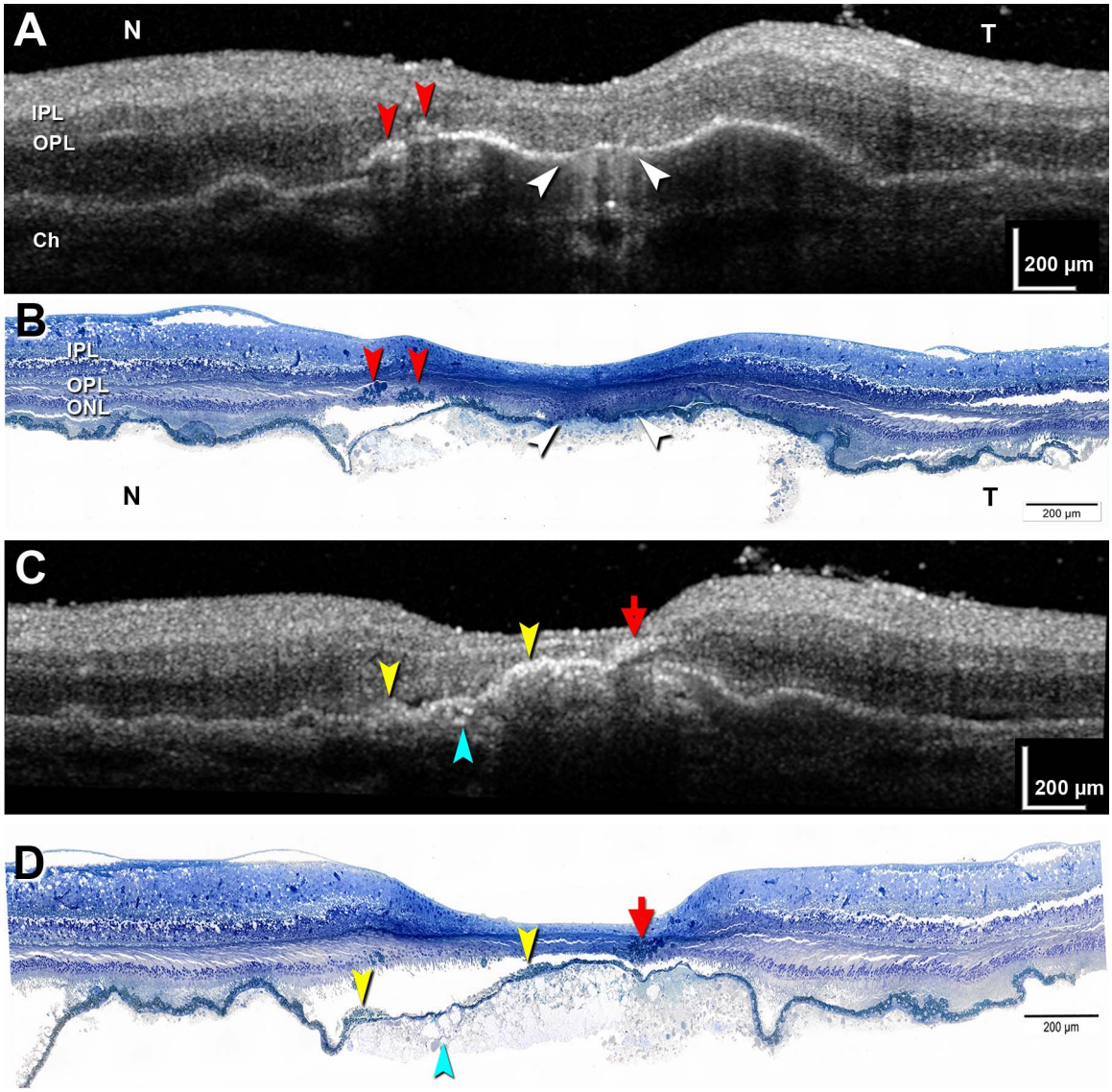


**Figure 5.** Correlations between ex vivo SDOCT and high-resolution histology in drusenoid pigment epithelium detachment. Matched pairs of SDOCT scans and histologic sections. Submicrometer epoxy resin sections of OTAP-postfixed specimens and toluidine blue stain. (**A**, **B**) Hypertransmission is associated with atrophy and dissociated RPE (*white arrowhead*). Two groups of intraretinal RPE cells are apparent (*red arrowheads*). (**C**, **D**) An RPE plume is created by a group of RPE cells tracking among the Henle fibers (*red arrow*). Hyperreflective material internal to the RPE layer represents a vitelliform lesion (*yellow arrowheads*). Calcium phosphate nodules are present (*teal arrowhead*). Ch, choroid; IPL, inner plexiform layer; ONL, outer nuclear layer; OPL, outer plexiform layer. Modified from Balaratnasingam C, Messinger JD, Sloan KR, Yannuzzi LA, Freund KB, Curcio CA. Histologic and optical coherence tomographic correlates in drusenoid pigment epithelium detachment in age-related macular degeneration. *Ophthalmology*. 2017;124:644–656. © 2017 by the American Academy of Ophthalmology.

## Some Hyperreflective Foci May Be Microglia

Hyperreflective foci in neovascular AMD and diabetic macula edema have been analyzed for size, reflectivity, and association with other signs of exudation like microaneurysms and hard exudates, prompting a hypothesis, predating our recent studies, that these foci represent microglia[19,20] migrating from inner to outer retina, as they do in degenerations and injuries.[82] This concept is supported by our ex vivo SDOCT imaging–histology correlations in two cases of PED associated with neovascular AMD,[12] We found that associated with intraretinal cysts were additional hyperreflective cells that were not RPE. The non-RPE cells were larger than RPE, spherical, and full of lipid droplets visualizable by OTAP post fixation and distinguishable from RPE organelles. Because a population of nonpigmented cells has not been reported in the subretinal space of aged human eyes (unlike mouse),[83] the lipid-filled cells are likely microglia. We hypothesize that anteriorly migrating RPE constitute one population of hyperreflective spots and posteriorly migrating lipid-filled microglia another, the latter active in clearing exuded plasma lipids. Interestingly, microglia in vitro take up 7-ketocholesterol, a proinflammatory oxysterol, and form intracellular lipid droplets.[84] If this hypothesis is true, RPE and microglia should be separable by size, clumping, motility, and multimodal imaging characteristics in studies of appropriate patients.[19,20,85,86] Further, of hyperreflective foci presaging type 3 (intraretinal) neovascularization, some lack flow signal on OCT angiography and thus are also likely cells.[87]

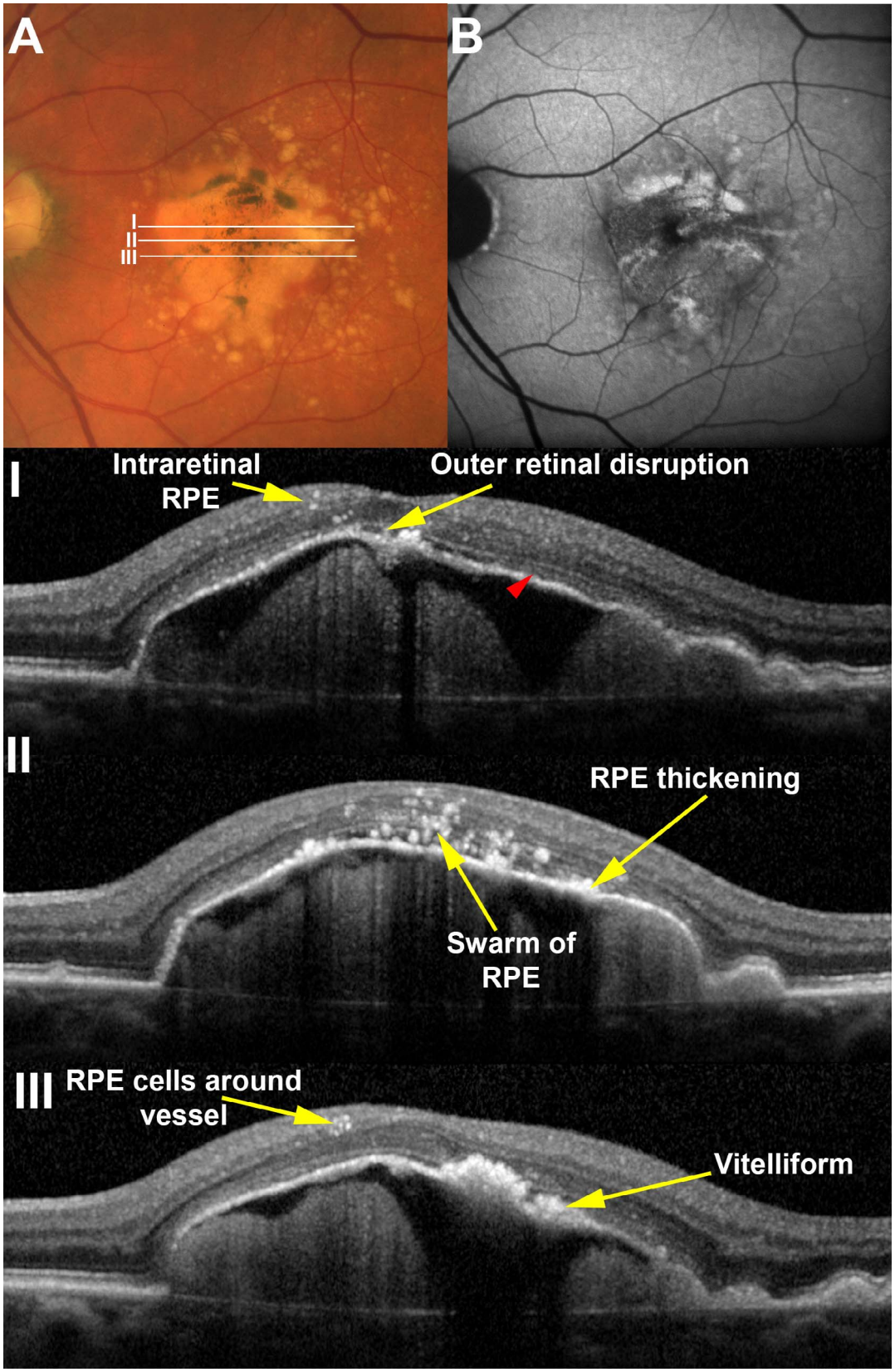


**Figure 6.** Histologically defined RPE features are visible in vivo. (**A**) A large drusenoid pigment epithelial detachment (DPED) in a 77-year-old male demonstrates pigmentary changes on the surface that correlate to (**B**) sites of increased fundus autofluorescence. Areas of B-scans (I–III) are illustrated in the color image. A range of RPE-related changes is seen on SDOCT scans including intraretinal RPE cells and vitelliform lesions. The ellipsoid zone (*red arrowhead*) is visible on the surface of the DPED except for at the apex, where it is notably absent. Although it was possible to distinguish vitelliform lesions from RPE thickening here, this distinction was not possible in all eyes examined. Reprinted from Balaratnasingam C, Messinger JD, Sloan KR, Yannuzzi LA, Freund KB, Curcio CA. Histologic and optical coherence tomographic correlates in drusenoid pigment epithelium detachment in age-related macular degeneration. *Ophthalmology.* 2017;124:644–656. © 2017 by the American Academy of Ophthalmology.

### Timing and Mechanism of RPE Activation With Respect to the Drusen Life Cycle

Longitudinal clinical imaging informed by histology can now establish a temporal sequence of cellular events preceding atrophy in drusenoid PED.[18] Following a thickening of the reflective RPE-BL band at baseline, hyperreflective foci appeared directly above in the retina several months later, supporting intraretinal RPE migration in vivo. For non-RPE cells to account for these phenomena, they must match both the organelle population and reflectivity of epithelial RPE and the spatiotemporal sequence of appearing in position, precisely over, and after, disturbances of the RPE layer.

Sarks et al.[88] demonstrated drusen coalescence and disappearance using serial fluorescein angiography, and druse dynamism has since been reinforced by several SDOCT datasets.[57,89] Drusen have a defined life cycle of net expansion over time, followed by collapse. Our group[14] established a life cycle of large drusenoid PED, using a Cavalieri method to measure PED volume over periods of up to 6.6 years. Although variable in rate across individuals, drusenoid PED followed a consistent pattern of a period of slow growth (0.022 $mm^3$/mo) followed by rapid collapse (0.199 $mm^3$/mo) (Fig. 7A). Intraretinal hyperreflective foci and acquired vitelliform lesions appeared just before the collapse. Importantly, the RPE-BL band became disrupted with streaks of hypertransmission preferentially at the druse apex, around the time of the collapse (Fig. 7B), and not at the PED base, where RPE tears begin. Not all PED end in complete collapse, as in some eyes the RPE dies leaving a raised plateau of persistent BLamD that becomes newly reflective with its RPE covering gone (Fig. 8; Supplementary Video S1). Even in this situation, however, RPE cells on the druse apex activate and migrate anteriorly, with the layer breaking up (Figs. 8C1, 8C2) and then disappearing, at which point persistent BLamD is apparent (Figs. 8C3, 8C4).

Further, strong experimental confirmation of a hypothesis of how soft drusen form can be combined with this new knowledge about RPE activation. In brief, a testable hypothesis for ultrastructural and molecular precursor pathways to soft drusen and basal linear deposit (BLinD) has been articulated based on multiple evidence lines.[90–94] These deposits are proposed as a downstream consequence to the dietary delivery of lipophilic essentials (vitamin A, lutein/zeaxanthin, vitamin E) to macular cells (photoreceptors, Müller cells, RPE) and the recycling of unneeded lipids, by RPE, to the circulation via lipoprotein particles containing apolipoproteins B and E.[91,93,94] One prediction of this hypothesis is that well-differentiated and polarized RPE cells could generate lipid-rich sub-RPE deposits in the absence of photoreceptors, as now demonstrated.[95,96] Human fetal RPE cells fed only standard culture medium basolaterally secrete apolipoprotein E–immunoreactive lipoprotein-like particles.[95] Further, primary porcine RPE grown on a resistive substrate establish a continuous layer of solid electron-dense material with histochemical and spectroscopic signatures of lipid and hydroxyapatite (calcium phosphate), conspicuously capturing both the initiation and progression of soft drusen.[96]

The combination of information about drusen formation, PED life cycle, and RPE phenotypes makes it possible to discern the spatiotemporal characteristics and significance of RPE cell death over drusen. If a druse is growing, the RPE is apparently functional enough to secrete lipoproteins and other druse components, which then back up against Bruch's membrane.[96] During this time, RPE cells on the druse apex either migrate into the retina or die, and the druse collapses, because the RPE is not present to maintain it. With the RPE gone, photoreceptors die too. It has been widely thought that as drusen collapse, the RPE dies, but it is really the contrary. First deduced by Arnold et al. from color photography and fluorescein angiography 20 years ago,[97] this sequence of events is now clear in longitudinal eye-tracked SDOCT. In a recent clinical trial of high-dose atorvastatin, Vavvas et al.[98] showed reduction of large drusen and less activated RPE over druse domes, consistent with this model.

RPE tend strongly to migrate anteriorly, suggesting either attractive signals from the retina or repellent signals from the druse or both. One explanation is that cells at the druse apex are at maximum distance from the choriocapillaris and thus migrate into retina to seek oxygen from retinal vessels. We considered the possibility that high mechanical tension on the RPE layer at the druse apex might serve to eject RPE cells; if this were true, RPE migration might occur more often in serous PED where such forces are presumably greater than in drusenoid PED. Our spatiotemporal data strongly support a model of RPE cell death focused on micronutrient deficiency, hypoxia, and bioenergetic failure related to distance from the choriocapillaris. Further, we can cautiously extrapolate from data on drusenoid PED to soft drusen in general, because drusenoid PED are the largest deposits on an established continuum leading to GA. In clinical studies using color fundus photography,[72,99] the formation of GA is consistently preceded by large drusen, then hyperpigmentation.[80] A life cycle similar to that of large drusenoid PED (Fig. 7) was also demonstrated for >6,000 RPE elevations of varying sizes with overlying hyperreflective foci by Schlanitz et al.[100] using automated OCT segmentation. Importantly, the SDOCT signatures of nascent GA developing over drusen domes[101] include a "break in the ELM," which is topologically equivalent to two curved descents of the ELM on either side of the druse apex, as illustrated (Fig. 26[72]; Fig. 3B[18]). Thus, the behavior of activated RPE migrating anteriorly and Müller cells concurrently scrolling up photoreceptors appear similar atop PED and at GA borders. Other theories of AMD pathogenesis such as impaired autophagy, oxidative stress, and systemic inflammation have yet to explain the precise localization and timing of RPE activation and death, in coordination with nearby photoreceptors and glia.

## Discussion

### Implications for Pathogenesis, Therapies, and Model Systems

These results in toto have important implications for theories of molecular pathogenesis. The identity of subretinal pigmented cells in various conditions has been debated for decades, with the two leading contenders RPE and either macrophages (bone marrow origin) or microglia (yolk sac origin)[102,103] that phagocytized RPE and retained characteristic RPE organelles. Transdifferentiation is the conversion of one differentiated cell type to another. In AMD, RPE is proposed to transdifferentiate to phenotypes with new behaviors, including motility[85] and expression of inflammatory markers. RPE cells in the anterior migratory pathway express CD163,[104] a marker of activated macrophages, and cells remaining in the RPE layer lose characteristic RPE markers.[105] Cells resembling subducted as well as cells in the RPE layer express CCR2 and CD18, a monocyte marker.[106] A transdifferentiation framework can incorporate immune functions newly acquired by RPE. Indeed, macrophages have long served as biological role models for RPE due to the commonality of phagocytosis.[107] Whether subretinal and intraretinal cells with melanosomes are macrophages/microglia, RPE expressing markers of these cells, or a mixture of

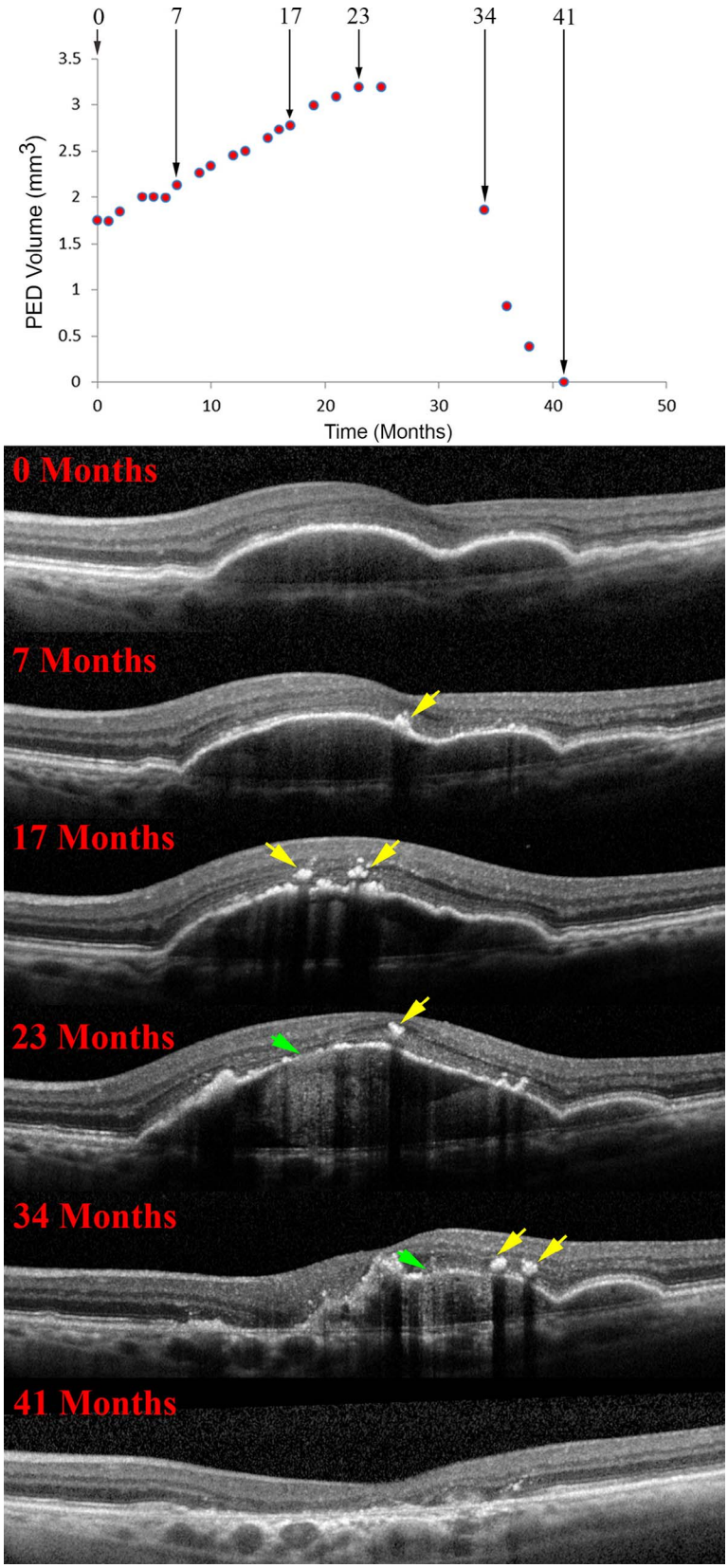


**Figure 7.** RPE morphology and the life cycle of drusenoid pigment epithelial detachment (DPED). (**A**) DPED volume as a function of time in a 72-year-old patient. Lines of best fit (*red*) were determined by piece-wise linear regression analysis. At 23 months after baseline the slope changes sharply from positive to negative. The rate of growth was slower than the rate of collapse in this illustrative case and all others in this series. (**B**) RPE changes in relationship to the DPED life cycle, as revealed by SDOCT. Intraretinal hyperreflective foci are first noted at 7 months as a localized hyperreflective lesion arising from the RPE-BL band (*yellow arrows*). At 23 months, disruptions to the RPE-BL band (*green arrow*) with increased light transmission (hypertransmission) to the choroid are evident, followed by a relatively rapid reduction in DPED volume until 41 months. Reprinted from Balaratnasingam C, Yannuzzi LA, Curcio CA, et al. Associations between retinal pigment epithelium and drusen volume changes during the life cycle of large drusenoid pigment epithelial detachments. *Invest Ophthalmol Vis Sci.* 2016;57:5479–5489, available under the CC BY-NC-ND license.

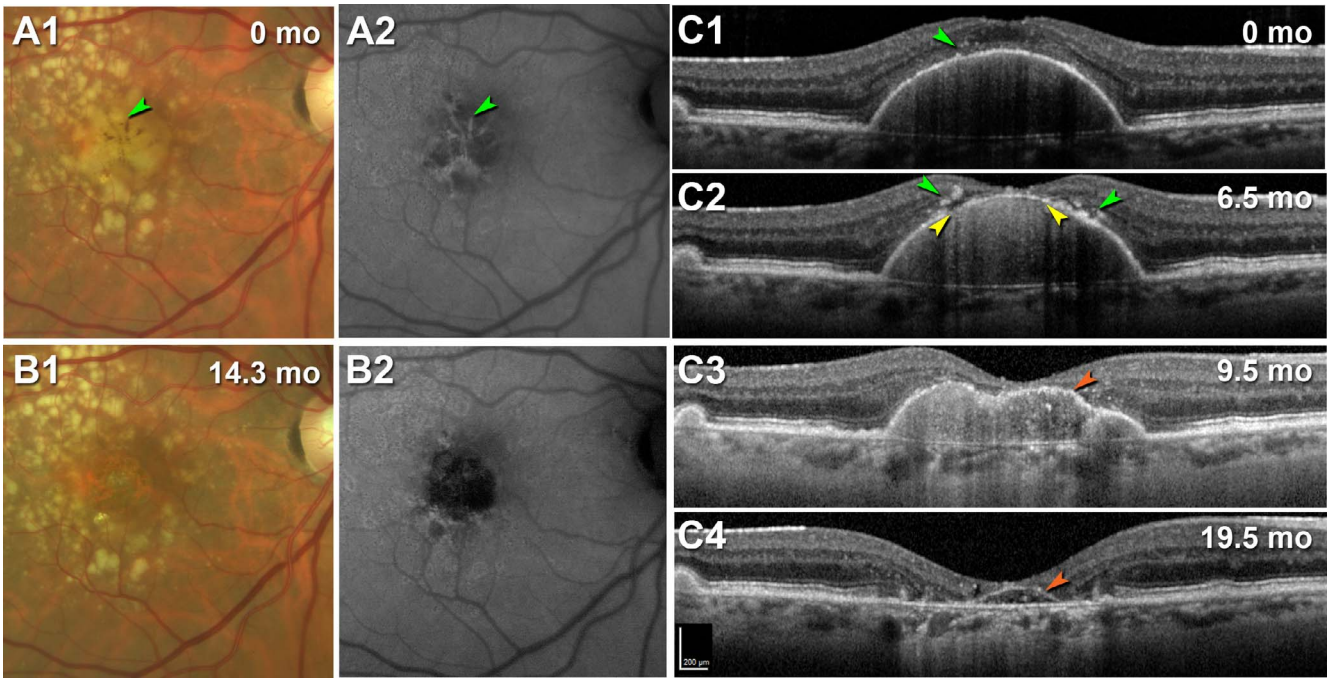


**Figure 8.** RPE activation and migration in the progression of drusenoid pigment epithelial detachment (DPED) to atrophy. Right eye of a 79-year-old woman with a large DPED. (**A1**, **B1**) Color fundus photography, (**A2**, **B2**) fundus autofluorescence with an excitation filter with a band pass range from 535 to 585 nm and a matched barrier filter with a band pass range of 605 to 715 nm.[23] (**C1–C4**) SDOCT at indicated time points. For SDOCT and near-infrared reflectance images at 16 intervals from baseline to 19.5 months (mo) see Supplementary Video S1. *Scale bar* in (**C4**) applies to (**C1–C4**). (**A1**, **A2**) At baseline, numerous drusen are apparent, including confluent soft drusen in the central macula with linear streaks of hyperpigmentation and hyperautofluorescence (*green arrowheads*). (**B1**, **B2**) Beginning at 3.5 months after baseline (see Supplementary Video S1), and very clear at 14.3 months, is the disappearance of the central confluent drusen, leaving a circular area of atrophy. (**C1–C4**) B-scans show a large drusenoid DPED with small hyperreflective foci at baseline that by 6.5 months has larger foci on either side of the apex (*green arrowheads*) where a thinned RPE-BL band and loss of overlying photoreceptor bands are associated with hypertransmission (*yellow arrowheads*). By 9.5 months, the RPE-BL band has thinned markedly due to loss of the cells, and at 19.5 months, this thin band persists as a plateau sign (*orange arrowheads*).

both, is a critical question. The answer impacts clinical image interpretation, therapeutic strategies, and choice of experimental model systems. Our data strongly tip the balance toward RPE origin in atrophic AMD.

These results inform therapeutic strategies first by indicating multiple pathways of RPE fate that may be differentially responsive to specific interventions. To the previously described major pathways of anterior migration and shedding, we can now add organelle expulsion (via vitelliform), hypothesizing that shedding and vitelliform represent molecularly distinct forms of cell death. This hypothesis is testable via immunolabeling studies to localize key markers for apoptosis, necroptosis, and autophagy inter alia in eyes specifically prepared for this purpose. Further, as cytoprotective or trophic RPE support via cell-based therapy is contemplated,[108,109] the multiple stress responses implied by different RPE phenotypes strongly motivate better understanding of the complex microenvironments that new cells will encounter. Lastly, paired histology and longitudinal imaging show that these pathways can be strongly linked to a common pathology, that is, the presence of drusen, suggesting that targeting drusen[98,110] may ameliorate or prevent RPE cell death in GA, along all pathways.

In research using animal models, the hypothesized origin of hyperreflective foci dictates the design of experiments. Molecularly diverse genetically engineered mouse models with deficient regulation of extracellular matrix, iron transport, mitochondria, cytoskeleton, and microRNA[111–116] exhibit pigmented cells in the subretinal space that the authors considered RPE, supporting anterior migration as a specific and repeatable stress response of RPE in vivo. Excellent SDOCT imaging is possible in mice, and some mouse models show hyperreflective foci.[116] In contrast, a vacuolated RPE phenotype is common in mice[117–123] and appears rarely in AMD macula.[6] Thus, therapies based on abating or eliminating this phenotype may have limited success in AMD patients.

## Histologically Informed SDOCT Metrics Can Now Be Tested

Our recent research has for the first time systematized RPE morphology, much seen previously, as hypotheses about biologic processes testable by future research, especially using clinical imaging. Our survey of RPE morphology has strengths (large number of advanced AMD eyes, unbiased systematic sampling, and high-resolution histology and photomicroscopy) and weaknesses (limited clinical histories including information about specific GA phenotypes,[75] biases in the distribution of the sample eyes, restriction to perikaryal morphology, and lack of molecular phenotyping due to glutaraldehyde fixation). Nonetheless, by combining the snapshot of quantitative, high-resolution histology with the movie of longitudinal multimodal imaging based on SDOCT, we gain important new insights about RPE fates in AMD while also validating RPE activation and migration as hyperreflective foci and thickening of the RPE-BL-Bruch's membrane band as biomarkers for progression. The availability of standardized SDOCT imaging in clinical trials and practices means that end stages can be tracked backward to impart new significance to earlier stages.[124–129] We can see the behavior of single RPE in

Investigative Ophthalmology & Visual Science

SDOCT, and activities may be watched in vivo for an accurate timeline and mapping of disease progression to provide a firm structural basis for future molecular assays. Because the human macula is precisely organized by layer and region, histologically validated SDOCT holds great promise for better understanding, wiser counsel to patients, and new therapies, as previously missing pieces of AMD are filled in for ever-greater clarity.

## *Acknowledgments*

The authors thank Jeffrey D. Messinger, DC, for assembling Figures 1 and 3 and performing the histology. The authors also thank David Fisher for designing Figure 4.

Presented at the Massachusetts Eye and Ear Infirmary–Schepens Eye Research Institute AMD Symposium, Boston, MA, USA, October 2016.

Supported by National Eye Institute (EY06109, P30 EY003039) for the acquisition of donor eyes, International Retinal Research Foundation, and the Arnold and Mabel Beckman Initiative for Macular Research. The Project MACULA Web site was supported by these and additionally by the Edward N. and Della L. Thome Memorial Foundation. The Eye Donor Project is supported by the Macula Foundation. C. A. Curcio is supported by the International Retinal Research Foundation, unrestricted funds to the Department of Ophthalmology from Research to Prevent Blindness, Inc., and EyeSight Foundation of Alabama.

Disclosure: **C.A. Curcio**, Novartis (C), Janssen Cell Therapy (C), Hoffman-LaRoche (F), Heidelberg Engineering (F); **E.C. Zanzottera**, None; **T. Ach**, Novartis (C); **C. Balaratnasingam**, None; **K.B. Freund**, Genentech (C, F), Optos (C), Optovue (C), Heidelberg Engineering (C), Graybug Vision (C)

## *References*

1. Wong WL, Su X, Li X, et al. Global prevalence of age-related macular degeneration and disease burden projection for 2020 and 2040: a systematic review and meta-analysis. *Lancet Glob Health*. 2014;2:e106–e116.
2. Maguire MG, Martin DF, Ying GS, et al. Five-year outcomes with anti-vascular endothelial growth factor treatment of neovascular age-related macular degeneration: the Comparison of Age-Related Macular Degeneration Treatments Trials. *Ophthalmology*. 2016;123:1751–1761.
3. Holz FG, Sadda S, Staurenghi G, et al. Imaging protocols for clinical studies in age-related macular degeneration – recommendations from Classification of Atrophy (CAM) Consensus Meeting. *Ophthalmology*. 2017;124:464–478.
4. Ooto S, Vongkulsiri S, Sato T, Suzuki M, Curcio CA, Spaide RF. Outer retinal corrugations in age-related macular degeneration. *JAMA Ophthalmol*. 2014;132:806–813.
5. Curcio CA, Balaratnasingam C, Messinger JD, Yannuzzi LA, Freund KB. Correlation of type 1 neovascularization associated with acquired vitelliform lesion in the setting of age-related macular degeneration. *Am J Ophthalmol*. 2015; 160:1024–1033.e3.
6. Zanzottera EC, Messinger JD, Ach T, Smith RT, Freund KB, Curcio CA. The Project MACULA retinal pigment epithelium grading system for histology and optical coherence tomography in age-related macular degeneration. *Invest Ophthalmol Vis Sci*. 2015;56:3253–3268.
7. Curcio CA, Messinger JD, Sloan KR, McGwin G Jr, Medeiros NE, Spaide RF. Subretinal drusenoid deposits in non-neovascular age-related macular degeneration: morphology, prevalence, topography, and biogenesis model. *Retina*. 2013;33:265–276.
8. Schaal KB, Freund KB, Litts KM, Zhang Y, Messinger JD, Curcio CA. Outer retinal tubulation in advanced age-related macular degeneration: optical coherence tomographic findings correspond to histology. *Retina*. 2015;35:1339–1350.
9. Litts KM, Messinger JD, Zhang Y, Freund KB, Curcio CA. Inner segment remodeling and mitochondrial translocation in degenerating cones of age-related macular degeneration, including outer retinal tubulation. *Invest Ophthalmol Vis Sci*. 2015;56:2243–2253.
10. Rudolf M, Vogt SD, Curcio CA, et al. Histologic basis of variations in retinal pigment epithelium autofluorescence in eyes with geographic atrophy. *Ophthalmology*. 2013;120: 821–828.
11. Ach T, Tolstik E, Messinger JD, Zarubina AV, Heintzmann R, Curcio CA. Lipofuscin re-distribution and loss accompanied by cytoskeletal stress in retinal pigment epithelium of eyes with age-related macular degeneration. *Invest Ophthalmol Vis Sci*. 2015;56:3242–3252.
12. Pang C, Messinger JD, Zanzottera EC, Freund KB, Curcio CA. The Onion Sign in neovascular age-related macular degeneration represents cholesterol crystals. *Ophthalmology*. 2015;122:2316–2326.
13. Zanzottera EC, Messinger JD, Ach T, Smith RT, Curcio CA. Subducted and melanotic cells in advanced age-related macular degeneration are derived from retinal pigment epithelium. *Invest Ophthalmol Vis Sci*. 2015;56:3269–3278.
14. Balaratnasingam C, Yannuzzi LA, Curcio CA, et al. Associations between retinal pigment epithelium and drusen volume changes during the lifecycle of large drusenoid pigment epithelial detachments. *Invest Ophthalmol Vis Sci*. 2016;57:5479–5489.
15. Chen KC, Jung JJ, Curcio CA, et al. Intraretinal hyperreflective foci in acquired vitelliform lesions of the macula: clinical and histologic study. *Am J Ophthalmol*. 2016;164: 89–98.
16. Zanzottera EC, Ach T, Huisingh C, Messinger JD, Freund KB, Curcio CA. Visualizing retinal pigment epithelium phenotypes in the transition to atrophy in neovascular age-related macular degeneration. *Retina*. 2016;36(suppl 1):S26–S39.
17. Zanzottera EC, Ach T, Huisingh C, Messinger JD, Spaide RF, Curcio CA. Visualizing retinal pigment epithelium phenotypes in the transition to geographic atrophy in age-related macular degeneration. *Retina*. 2016;36(suppl 1):S12–S25.
18. Balaratnasingam C, Messinger JD, Sloan KR, Yannuzzi LA, Freund KB, Curcio CA. Histology and optical coherence tomographic correlations in drusenoid pigment epithelium detachment in age-related macular degeneration. *Ophthalmology*. 2017;124:644–656.
19. Vujosevic S, Bini S, Torresin T, et al. Hyperreflective retinal spots in normal and diabetic eyes: B-scan and en face spectral domain optical coherence tomography evaluation. *Retina*. 2017;37:1092–1103.
20. Coscas G, De Benedetto U, Coscas F, et al. Hyperreflective dots: a new spectral-domain optical coherence tomography entity for follow-up and prognosis in exudative age-related macular degeneration. *Ophthalmologica*. 2013;229:32–37.
21. Fleckenstein M, Charbel Issa P, Helb HM, et al. High-resolution spectral domain-OCT imaging in geographic atrophy associated with age-related macular degeneration. *Invest Ophthalmol Vis Sci*. 2008;49:4137–4144.
22. Göbel AP, Fleckenstein M, Schmitz-Valckenberg S, Brinkmann CK, Holz FG. Imaging geographic atrophy in age-related macular degeneration. *Ophthalmologica*. 2011;226: 182–190.
23. Spaide RF, Curcio CA. Drusen characterization with multimodal imaging. *Retina*. 2010;30:1441–1454.
24. Curcio CA, Sloan KR, Kalina RE, Hendrickson AE. Human photoreceptor topography. *J Comp Neurol*. 1990;292:497–523.

25. Curcio CA, Allen KA. Topography of ganglion cells in human retina. *J Comp Neurol*. 1990;300:5–25.
26. Scoles D, Sulai Y, Langlo C, et al. In vivo imaging of human cone photoreceptor inner segments. *Invest Ophthalmol Vis Sci*. 2014;55:4244–4251.
27. Zhang T, Godara P, Blanco ER, et al. Variability in human cone topography assessed by adaptive optics scanning laser ophthalmoscopy. *Am J Ophthalmol*. 2015;160:290–300.e1.
28. Rossi EA, Granger CE, Sharma R, et al. Imaging individual neurons in the retinal ganglion cell layer of the living eye. *Proc Natl Acad Sci U S A*. 2017;114:586–591.
29. Toth CA, Narayan DG, Boppart SA, et al. A comparison of retinal morphology viewed by optical coherence tomography and by light microscopy. *Arch Ophthalmol*. 1997;115:1425–1428.
30. Yabushita H, Bouma BE, Houser SL, et al. Characterization of human atherosclerosis by optical coherence tomography. *Circulation*. 2002;106:1640–1645.
31. Cilingiroglu M, Oh JH, Sugunan B, et al. Detection of vulnerable plaque in a murine model of atherosclerosis with optical coherence tomography. *Catheter Cardiovasc Interv*. 2006;67:915–923.
32. Gambichler T, Moussa G, Regeniter P, et al. Validation of optical coherence tomography in vivo using cryostat histology. *Phys Med Biol*. 2007;52:N75–N85.
33. Drexler W, Fujimoto JG. State-of-the-art retinal optical coherence tomography. *Prog Retin Eye Res*. 2008;27:45–88.
34. Huang Y, Cideciyan AV, Papastergiou GI, et al. Relation of optical coherence tomography to microanatomy in normal and rd chickens. *Invest Ophthalmol Vis Sci*. 1998;39:2405–2416.
35. Fischer MD, Huber G, Beck SC, et al. Noninvasive, in vivo assessment of mouse retinal structure using optical coherence tomography. *PLoS One*. 2009;4:e7507.
36. Srinivasan VJ, Ko TH, Wojtkowski M, et al. Noninvasive volumetric imaging and morphometry of the rodent retina with high-speed, ultrahigh-resolution optical coherence tomography. *Invest Ophthalmol Vis Sci*. 2006;47:5522–5528.
37. Gloesmann M, Hermann B, Schubert C, Sattmann H, Ahnelt PK, Drexler W. Histologic correlation of pig retina radial stratification with ultrahigh-resolution optical coherence tomography. *Invest Ophthalmol Vis Sci*. 2003;44:1696–1703.
38. Abbott CJ, McBrien NA, Grunert U, Pianta MJ. Relationship of the optical coherence tomography signal to underlying retinal histology in the tree shrew (Tupaia belangeri). *Invest Ophthalmol Vis Sci*. 2009;50:414–423.
39. Chauhan DS, Marshall J. The interpretation of optical coherence tomography images of the retina. *Invest Ophthalmol Vis Sci*. 1999;40:2332–2342.
40. Chen TC, Cense B, Miller JW, et al. Histologic correlation of in vivo optical coherence tomography images of the human retina. *Am J Ophthalmol*. 2006;141:1165–1168.
41. Ghazi NG, Dibernardo C, Ying HS, Mori K, Gehlbach PL. Optical coherence tomography of enucleated human eye specimens with histological correlation: origin of the outer "red line." *Am J Ophthalmol*. 2006;141:719–726.
42. Brown NH, Koreishi AF, McCall M, Izatt JA, Rickman CB, Toth CA. Developing SDOCT to assess donor human eyes prior to tissue sectioning for research. *Graefes Arch Clin Exp Ophthalmol*. 2009;247:1069–1080.
43. Spaide R, Curcio CA. Anatomic correlates to the bands seen in the outer retina by optical coherence tomography: literature review and model. *Retina*. 2011;31:1609–1619.
44. Sarks SH, Arnold JJ, Sarks JP, Gilles MC, Walter CJ. Prophylactic perifoveal laser treatment of soft drusen. *Aust N Z J Ophthalmol*. 1996;24:15–26.
45. Klein R, Klein BE, Tomany SC, Meuer SM, Huang GH. Ten-year incidence and progression of age-related maculopathy: The Beaver Dam eye study. *Ophthalmology*. 2002;109:1767–1779.
46. Klein R, Klein BE, Knudtson MD, Meuer SM, Swift M, Gangnon RE. Fifteen-year cumulative incidence of age-related macular degeneration: the Beaver Dam Eye Study. *Ophthalmology*. 2007;114:253–262.
47. Joachim ND, Mitchell P, Kifley A, Wang JJ. Incidence, progression, and associated risk factors of medium drusen in age-related macular degeneration: findings from the 15-year follow-up of an Australian cohort. *JAMA Ophthalmol*. 2015;133:698–705.
48. Pieroni CG, Witkin AJ, Ko TH, et al. Ultrahigh resolution optical coherence tomography in non-exudative age related macular degeneration. *Br J Ophthalmol*. 2006;90:191–197.
49. Schuman SG, Koreishi AF, Farsiu S, Jung SH, Izatt JA, Toth CA. Photoreceptor layer thinning over drusen in eyes with age-related macular degeneration imaged in vivo with spectral-domain optical coherence tomography. *Ophthalmology*. 2009;116:488–496.e2.
50. Keane PA, Patel PJ, Liakopoulos S, Heussen FM, Sadda SR, Tufail A. Evaluation of age-related macular degeneration with optical coherence tomography. *Surv Ophthalmol*. 2012;57:389–414.
51. Zacks DN, Johnson MW. Transretinal pigment migration: an optical coherence tomographic study. *Arch Ophthalmol*. 2004;122:406–408.
52. Ho J, Witkin AJ, Liu J, et al. Documentation of intraretinal retinal pigment epithelium migration via high-speed ultra-high-resolution optical coherence tomography. *Ophthalmology*. 2011;118:687–693.
53. Folgar FA, Chow JH, Farsiu S, et al. Spatial correlation between hyperpigmentary changes on color fundus photography and hyperreflective foci on SDOCT in intermediate AMD. *Invest Ophthalmol Vis Sci*. 2012;53:4626–4633.
54. Ouyang Y, Heussen FM, Hariri A, Keane PA, Sadda SR. Optical coherence tomography-based observation of the natural history of drusenoid lesion in eyes with dry age-related macular degeneration. *Ophthalmology*. 2013;120:2656–2665.
55. Christenbury JG, Folgar FA, O'Connell RV, Chiu SJ, Farsiu S, Toth CA. Progression of intermediate age-related macular degeneration with proliferation and inner retinal migration of hyperreflective foci. *Ophthalmology*. 2013;120:1038–1045.
56. Lei J, Balasubramanian S, Abdelfattah NS, Nittala M, Sadda SR. Proposal of a simple optical coherence tomography-based scoring system for progression of age related macular degeneration [published online ahead of print May 22, 2017]. *Graefes Arch Clin Exp Ophthalmol*. doi:10.1007/s00417-017-3693-y.
57. Yehoshua Z, Wang F, Rosenfeld PJ, Penha FM, Feuer WJ, Gregori G. Natural history of drusen morphology in age-related macular degeneration using spectral domain optical coherence tomography. *Ophthalmology*. 2011;118:2434–2441.
58. Zweifel SA, Imamura Y, Spaide TC, Fujiwara T, Spaide RF. Prevalence and significance of subretinal drusenoid deposits (reticular pseudodrusen) in age-related macular degeneration. *Ophthalmology*. 2010;117:1775–1781.
59. Guyton JR, Klemp KF. Ultrastructural discrimination of lipid droplets and vesicles in atherosclerosis: value of osmium-thiocarbohydrazide-osmium and tannic acid-paraphenylenediamine techniques. *J Histochem Cytochem*. 1988;36:1319–1328.
60. Curcio CA, Millican CL, Bailey T, Kruth HS. Accumulation of cholesterol with age in human Bruch's membrane. *Invest Ophthalmol Vis Sci*. 2001;42:265–274.


Investigative Ophthalmology & Visual Science

61. Curcio CA, Presley JB, Millican CL, Medeiros NE. Basal deposits and drusen in eyes with age-related maculopathy: evidence for solid lipid particles. *Exp Eye Res*. 2005;80:761–775.
62. Jiang M, Esteve-Rudd J, Lopes VS, et al. Microtubule motors transport phagosomes in the RPE, and lack of KLC1 leads to AMD-like pathogenesis. *J Cell Biol*. 2015;210:595–611.
63. Wilson JD, Cottrell WJ, Foster TH. Index-of-refraction-dependent subcellular light scattering observed with organelle-specific dyes. *J Biomed Opt*. 2007;12:014010.
64. Wilson JD, Foster TH. Characterization of lysosomal contribution to whole-cell light scattering by organelle ablation. *J Biomed Opt*. 2007;12:030503.
65. Wilson JD, Giesselman BR, Mitra S, Foster TH. Lysosome-damage-induced scattering changes coincide with release of cytochrome c. *Opt Lett*. 2007;32:2517–2519.
66. Staurenghi G, Sadda S, Chakravarthy U, Spaide RF. Proposed lexicon for anatomic landmarks in normal posterior segment spectral-domain optical coherence tomography: The IN*-OCT Consensus. *Ophthalmology*. 2014;121:1572–1578.
67. Balaratnasingam C, Hoang QV, Inoue M, et al. Clinical characteristics, choroidal neovascularization, and predictors of visual outcomes in acquired vitelliform lesions. *Am J Ophthalmol*. 2016;172:28–38.
68. Guidry C, Medeiros NE, Curcio CA. Phenotypic variation of retinal pigment epithelium in age-related macular degeneration. *Invest Ophthalmol Vis Sci*. 2002;43:267–273.
69. Vogt SD, Curcio CA, Wang L, et al. Retinal pigment epithelial expression of complement regulator CD46 is altered early in the course of geographic atrophy. *Exp Eye Res*. 2011;93:413–423.
70. Dolz-Marco R, Litts KM, Tan ACS, Freund KB, Curcio CA. The evolution of outer retinal tubulation, a neurodegeneration and gliosis prominent in macular diseases [published online ahead of print April 26, 2017]. *Ophthalmology*. doi: 10.1016/j.ophtha.2017.03.043.
71. Tan ACS, Astroz P, Dansingani KK, et al. The plateau, an optical coherence tomographic signature of geographic atrophy: evolution, multimodal imaging, and candidate histology. *Invest Ophthalmol Vis Sci*. 2017;58:2349–2358.
72. Sarks JP, Sarks SH, Killingsworth MC. Evolution of geographic atrophy of the retinal pigment epithelium. *Eye*. 1988;2:552–577.
73. Sarks SH. Ageing and degeneration in the macular region: a clinico-pathological study. *Br J Ophthalmol*. 1976;60:324–341.
74. Sarks J, Tang K, Killingsworth M, Arnold J, Sarks S. Development of atrophy of the retinal pigment epithelium around disciform scars. *Br J Ophthalmol*. 2006;90:442–446.
75. Holz FG, Bindewald-Wittich A, Fleckenstein M, Dreyhaupt J, Scholl HP, Schmitz-Valckenberg S. Progression of geographic atrophy and impact of fundus autofluorescence patterns in age-related macular degeneration. *Am J Ophthalmol*. 2007;143:463–472.
76. Schmitz-Valckenberg S, Sahel JA, Danis R, et al. Natural history of geographic atrophy progression secondary to age-related macular degeneration (Geographic Atrophy Progression study). *Ophthalmology*. 2016;123:361–368.
77. Casswell AG, Kohen D, Bird AC. Retinal pigment epithelial detachments in the elderly: classification and outcome. *Br J Ophthalmol*. 1985;69:397–403.
78. Hartnett ME, Weiter JJ, Garsd A, Jalkh AE. Classification of retinal pigment epithelial detachments associated with drusen. *Graefes Arch Clin Exp Ophthalmol*. 1992;230:11–19.
79. Roquet W, Roudot-Thoraval F, Coscas G, Soubrane G. Clinical features of drusenoid pigment epithelial detachment in age related macular degeneration. *Br J Ophthalmol*. 2004;88:638–642.
80. Cukras C, Agron E, Klein ML, et al. Natural history of drusenoid pigment epithelial detachment in age-related macular degeneration: Age-Related Eye Disease Study Report No. 28. *Ophthalmology*. 2010;117:489–499.
81. Mrejen S, Sarraf D, Mukkamala SK, Freund KB. Multimodal imaging of pigment epithelial detachment: a guide to evaluation. *Retina*. 2013;33:1735–1762.
82. Karlstetter M, Scholz R, Rutar M, Wong WT, Provis JM, Langmann T. Retinal microglia: just bystander or target for therapy? *Prog Retin Eye Res*. 2015;45:30–57.
83. Xu H, Chen M, Manivannan A, Lois N, Forrester JV. Age-dependent accumulation of lipofuscin in perivascular and subretinal microglia in experimental mice. *Aging Cell*. 2008;7:58–68.
84. Indaram M, Ma W, Zhao L, Fariss RN, Rodriguez IR, Wong WT. 7-ketocholesterol increases retinal microglial migration, activation, and angiogenicity: a potential pathogenic mechanism underlying age-related macular degeneration. *Sci Rep*. 2015;5:9144.
85. Gocho K, Sarda V, Falah S, et al. Adaptive optics imaging of geographic atrophy. *Invest Ophthalmol Vis Sci*. 2013;54:3673–3680.
86. Lammer J, Bolz M, Baumann B, et al. Detection and analysis of hard exudates by polarization-sensitive optical coherence tomography in patients with diabetic maculopathy. *Invest Ophthalmol Vis Sci*. 2014;55:1564–1571.
87. Tan AC, Dansingani KK, Yannuzzi LA, Sarraf D, Freund KB. Type 3 neovascularization imaged with cross-sectional and en face optical coherence tomography angiography. *Retina*. 2016;37:234–246.
88. Sarks JP, Sarks SH, Killingsworth MC. Evolution of soft drusen in age-related macular degeneration. *Eye*. 1994;8:269–283.
89. Schlanitz FG, Baumann B, Kundi M, et al. Drusen volume development over time and its relevance to the course of age-related macular degeneration. *Br J Ophthalmol*. 2016;101:198–203.
90. Spaide RF, Armstrong D, Browne R. Continuing medical education review: choroidal neovascularization in age-related macular degeneration–what is the cause? *Retina*. 2003;23:595–614.
91. Curcio CA, Johnson M, Huang J-D, Rudolf M. Aging, age-related macular degeneration, and the Response-to-Retention of apolipoprotein B-containing lipoproteins. *Prog Retin Eye Res*. 2009;28:393–422.
92. Curcio CA, Johnson M, Huang J-D, Rudolf M. Apolipoprotein B-containing lipoproteins in retinal aging and age-related maculopathy. *J Lipid Res*. 2010;51:451–467.
93. Curcio CA, Johnson M, Rudolf M, Huang J-D. The oil spill in ageing Bruch's membrane. *Br J Ophthalmol*. 2011;95:1638–1645.
94. Pikuleva I, Curcio CA. Cholesterol in the retina: the best is yet to come. *Prog Retin Eye Res*. 2014;41:64–89.
95. Johnson LV, Forest DL, Banna CD, et al. Cell culture model that mimics drusen formation and triggers complement activation associated with age-related macular degeneration. *Proc Natl Acad Sci U S A*. 2011;108:18277–18282.
96. Pilgrim M, Lengyel I, Lanzirotti A, et al. Sub-retinal pigment epithelial deposition of drusen components including hydroxyapatite in a primary cell culture model. *Invest Ophthalmol Vis Sci*. 2017;58:708–719.
97. Arnold JJ, Quaranta M, Soubrane G, Sarks SH, Coscas G. Indocyanine green angiography of drusen. *Am J Ophthalmol*. 1997;124:344–356.
98. Vavvas DG, Daniels AB, Kapsala ZG, et al. Regression of some high-risk features of age-related macular degeneration (AMD)


Investigative Ophthalmology & Visual Science

in patients receiving intensive statin treatment. *EBioMedicine*. 2016;5:198–203.

99. Klein ML, Ferris FL III, Armstrong J, et al. Retinal precursors and the development of geographic atrophy in age-related macular degeneration. *Ophthalmology*. 2008;115:1026–1031.
100. Schlanitz FG, Sacu S, Baumann B, et al. Identification of drusen characteristics in age-related macular degeneration by polarization-sensitive optical coherence tomography. *Am J Ophthalmol*. 2015;160:335–344.e1.
101. Wu Z, Luu CD, Ayton LN, et al. Optical coherence tomography-defined changes preceding the development of drusen-associated atrophy in age-related macular degeneration. *Ophthalmology*. 2014;121:2415–2422.
102. Alliot F, Godin I, Pessac B. Microglia derive from progenitors, originating from the yolk sac, and which proliferate in the brain. *Brain Res Dev Brain Res*. 1999;117:145–152.
103. Karlstetter M, Nothdurfter C, Aslanidis A, et al. Translocator protein (18 kDa) (TSPO) is expressed in reactive retinal microglia and modulates microglial inflammation and phagocytosis. *J Neuroinflammation*. 2014;11:3.
104. Lad EM, Cousins SW, Van Arnam JS, Proia AD. Abundance of infiltrating CD163+ cells in the retina of postmortem eyes with dry and neovascular age-related macular degeneration. *Graefes Arch Clin Exp Ophthalmol*. 2015;253:1941–1945.
105. Lad EM, Cousins SW, Proia AD. Identity of pigmented subretinal cells in age-related macular degeneration. *Graefes Arch Clin Exp Ophthalmol*. 2016;254:1239–1241.
106. Sennlaub F, Auvynet C, Calippe B, et al. CCR2(+) monocytes infiltrate atrophic lesions in age-related macular disease and mediate photoreceptor degeneration in experimental subretinal inflammation in Cx3cr1 deficient mice. *EMBO Mol Med*. 2013;5:1775–1793.
107. Steinberg RH. Interactions between the retinal pigment epithelium and the neural retina. *Doc Ophthalmol*. 1985;60:327–346.
108. Evans JB, Syed BA. New hope for dry AMD? *Nat Rev Drug Discov*. 2013;12:501–502.
109. Schwartz SD, Regillo CD, Lam BL, et al. Human embryonic stem cell-derived retinal pigment epithelium in patients with age-related macular degeneration and Stargardt's macular dystrophy: follow-up of two open-label phase 1/2 studies. *Lancet*. 2014;385:509–516.
110. Jobling AI, Guymer RH, Vessey KA, et al. Nanosecond laser therapy reverses pathologic and molecular changes in age-related macular degeneration without retinal damage. *FASEB J*. 2015;29:696–710.
111. Collin GB, Hubmacher D, Charette JR, et al. Disruption of murine Adamtsl4 results in zonular fiber detachment from the lens and in retinal pigment epithelium dedifferentiation. *Hum Mol Genet*. 2015;24:6958–6974.
112. Hahn P, Qian Y, Dentchev T, et al. Disruption of ceruloplasmin and hephaestin in mice causes retinal iron overload and retinal degeneration with features of age-related macular degeneration. *Proc Natl Acad Sci U S A*. 2004;101:13850–13855.
113. Zhao C, Yasumura D, Li X, et al. mTOR-mediated dedifferentiation of the retinal pigment epithelium initiates photoreceptor degeneration in mice. *J Clin Invest*. 2011;121:369–383.
114. Patil H, Saha A, Senda E, et al. Selective impairment of a subset of Ran-GTP-binding domains of ran-binding protein 2 (Ranbp2) suffices to recapitulate the degeneration of the retinal pigment epithelium (RPE) triggered by Ranbp2 ablation. *J Biol Chem*. 2014;289:29767–29789.
115. Saksens NT, Krebs MP, Schoenmaker-Koller FE, et al. Mutations in CTNNA1 cause butterfly-shaped pigment dystrophy and perturbed retinal pigment epithelium integrity. *Nat Genet*. 2016;48:144–151.
116. Sundermeier TR, Sakami S, Sahu B, et al. microRNA-processing enzymes are essential for survival and function of mature retinal pigmented epithelial cells in mice. *J Biol Chem*. 2017;292:3366–3378.
117. Hollyfield JG, Bonilha VL, Rayborn ME, et al. Oxidative damage-induced inflammation initiates age-related macular degeneration. *Nat Med*. 2008;14:194–198.
118. Zhao Z, Chen Y, Wang J, et al. Age-related retinopathy in NRF2-deficient mice. *PLoS One*. 2011;6:e19456.
119. Kleinman ME, Kaneko H, Cho WG, et al. Short-interfering RNAs induce retinal degeneration via TLR3 and IRF3. *Mol Ther*. 2012;20:101–108.
120. Hu P, Herrmann R, Bednar A, et al. Aryl hydrocarbon receptor deficiency causes dysregulated cellular matrix metabolism and age-related macular degeneration-like pathology. *Proc Natl Acad Sci U S A*. 2013;110:E4069–E4078.
121. Rowan S, Weikel KA, Chang ML, et al. Cfh genotype interacts with dietary glycemic index to modulate age-related macular degeneration-like features in mice. *Invest Ophthalmol Vis Sci*. 2013;55:492–501.
122. Mao H, Seo SJ, Biswal MR, et al. Mitochondrial oxidative stress in the retinal pigment epithelium leads to localized retinal degeneration. *Invest Ophthalmol Vis Sci*. 2014;55:4613–4627.
123. Shang P, Valapala M, Grebe R, et al. The amino acid transporter SLC36A4 regulates the amino acid pool in retinal pigmented epithelial cells and mediates the mechanistic target of rapamycin, complex 1 signaling. *Aging Cell*. 2017;16:349–359.
124. Moussa K, Lee JY, Stinnett SS, Jaffe GJ. Spectral domain optical coherence tomography-determined morphologic predictors of age-related macular degeneration-associated geographic atrophy progression. *Retina*. 2013;33:1590–1599.
125. Wu Z, Luu CD, Ayton LN, et al. Optical coherence tomography-defined changes preceding the development of drusen-associated atrophy in age-related macular degeneration. *Ophthalmology*. 2014;121:2415–2422.
126. Sayegh RG, Simader C, Scheschy U, et al. A systematic comparison of spectral-domain optical coherence tomography and fundus autofluorescence in patients with geographic atrophy. *Ophthalmology*. 2011;118:1844–1851.
127. Simader C, Sayegh RG, Montuoro A, et al. A longitudinal comparison of spectral-domain optical coherence tomography and fundus autofluorescence in geographic atrophy. *Am J Ophthalmol*. 2014;158:557–566.e1.
128. Grunwald JE, Daniel E, Huang J, et al. Risk of geographic atrophy in the Comparison of Age-related Macular Degeneration Treatments Trials. *Ophthalmology*. 2014;121:150–161.
129. Marsiglia M, Boddu S, Chen CY, et al. Correlation between neovascular lesion type and clinical characteristics of non-neovascular fellow eyes in patients with unilateral neovascular age-related macular degeneration. *Retina*. 2015;35:966–974.
130. Litts KM, Wang X, Clark ME, et al. Exploring photoreceptor reflectivity via multimodal imaging of outer retinal tubulation in advanced age-related macular degeneration. *Retina*. 2017;37:978–988.

Investigative Ophthalmology & Visual Science